New Layered Zirconium Tellurides: $Zr_{0.30}ZrTe_2$, $Zr_{0.29}Zr_2Te_2As$, and $NaZr_2Te_2As$

Chwanchin Wang, Cahit Eylem, and Timothy Hughbanks*

Department of Chemistry, P.O. Box 300012, Texas A&M University, College Station, Texas 77842-3012

Received July 24, 1997

The synthesis and crystal structure determinations of $Zr_{0.30}ZrTe_2$ and $M_xZr_2Te_2As$ (M = Zr, Na) compounds are reported. The structure of $Zr_{0.30}ZrTe_2$ was refined in the hexagonal space group $P6_3mc$ (No. 186, $Z = 2$) with lattice parameters $a = 3.9840(3)$ Å and $c = 13.366(3)$ Å; $Zr_{0.29}Zr_2Te_2As$ was refined in the rhombohedral space group $R\bar{3}m$ (No. 166, $Z = 3$) with lattice parameters $a = 3.9329(4)$ Å and $c = 29.564(5)$ Å. $Zr_{0.30}ZrTe_2$ and $Zr_{0.29}Zr_2Te_2As$ have close structural similarities to Zr_2Se_3 and Ta_2S_2C, respectively, and are built up by stacking hexagonal layers with [$Zr_{0.30}$−Te−Zr−Te] and [$Zr_{0.29}$−Te−Zr−As−Zr−Te] sequences. Four-probe resistivity measurements (77−300 K) show both $Zr_{0.30}ZrTe_2$ and $Zr_{0.29}Zr_2Te_2As$ to be metallic ($Zr_{0.29}Zr_2Te_2As$: 8.9×10^{-5} Ω cm at 273 K). Both compounds exhibit structures wherein Zr atoms are included between layers ($ZrTe_2$ and Zr_2Te_2As) by partially filling trigonal antiprismatic holes. The replacement of the included Zr ions in $Zr_{0.29}Zr_2Te_2As$ by Na ions has been demonstrated. Powder diffraction data showed that $NaZr_2Te_2As$ is isostructural with $Zr_{0.29}Zr_2Te_2As$. By use of Rietveld refinements, sodium ions were found to reside in the trigonal antiprismatic sites between the layers. Extended Hückel band calculations on the $[Zr_2Te_2As]^{1.16-}$ layer indicate that it should be a metallic conductor and that the [Zr_2Te_2As] layer can bear a greater negative charge than has so far been observed. We suggest that the [Zr_2Te_2As] layered compounds may offer new opportunities as electron-donating hosts.

Introduction

Guest−host interactions of low-dimensional transition metal chalcogenides have been extensively studied because of such compounds' unusual physical properties, interesting structural chemistry, and many applications.[1−5] Recently, much attention has been focused on the chemistry of ternary transition metal tellurides and, in particular, investigation of ternary layered group 5−M′−Te (M′ = 3d transition metals) systems have lately produced many interesting materials. Examples include $MM'Te_5$ (M = Nb, Ta; M′ = Ni, Pt),[6−9] $MIrTe_4$ (M = Ta, Nb),[10] $Ta_3Co_3Te_{14}$,[6] $Ta_4Co_3Te_{16}$,[11] $MM'Te_2$ (M = Nb, Ta; M′ = Fe, Co, Ni),[12−17] $Ta_{1.09}Fe_{2.39}Te_4$,[18] $Ta_2M_3Q_5$ (M = Ni, Pd; Q = Se, Te),[15,19,20] $TaCo_2Te_2$,[21] $TaFe_{1.25}Te_3$,[22] $TaNi_{2.05}Te_3$,[23] and $NbNi_{2.38}Te_3$.[24] The incorporation of main group elements has also been reported in MX_nTe_2 (M = Nb, Ta; X = Si, Ge; $^1/_3 < n < {}^1/_2$) materials.[25,26]

In contrast with these group 5 ternary layered tellurides, there have been comparatively few reports of the incorporation of ternary elements in Zr and Hf tellurides. $K_4M_3Te_{17}$ (M = Zr, Hf)[27] and $Cs_4Zr_3Te_{16}$,[28] which contain fully oxidized Zr or Hf, have been reported. The layered materials $MGeTe_4$ (M = Zr, Hf),[29] ZrXQ (X = Si, Ge, As, Sb; Q = S, Se, Te),[30−33] some

* Author to whom correspondence should be addressed.

(1) Hulliger, F. *Structural Chemistry of Layer-type Phases*; Reidel: Dordrecht, The Netherlands, 1976; Vol. 5.
(2) Rouxel, J.; Brec, R. *Annu. Rev. Mater. Sci.* **1986**, *16*, 137−162.
(3) Rouxel, J. *Crystal Chemistry and Properties of Materials with Quasi-one-dimensional Structures*; D. Reidel: Dordrecht, Holland, 1986.
(4) Schöllhorn, R. *Materials and Models: Faces of Intercalation Chemistry*; Schöllhorn, R., Ed.; Kluwer: Dordrecht, The Netherlands, 1994; Vol. 17, pp 1−82.
(5) Whittingham, M. S.; Ebert, L. B. *Applications of Intercalation Compounds*; Whittingham, M. S., Ebert, L. B., Eds.; D. Reidel: Dordrecht, Holland, 1979; pp 533−562.
(6) Mar, A.; Ibers, J. A. *J. Solid State Chem.* **1991**, *92*, 352−361.
(7) Liimatta, E. W.; Ibers, J. A. *J. Solid State Chem.* **1987**, *71*, 384−389.
(8) Liimatta, E. W.; Ibers, J. A. *J. Solid State Chem.* **1988**, *77*, 141−147.
(9) Liimatta, E. W.; Ibers, J. A. *J. Solid State Chem.* **1989**, *78*, 7−16.
(10) Mar, A.; Jobic, S.; Ibers, J. A. *J. Am. Chem. Soc.* **1992**, *114*, 8963−8971.
(11) Mar, A.; Ibers, J. A. *J. Chem. Soc., Dalton Trans.* **1991**, 639−641.
(12) Li, J.; Badding, M. E.; DiSalvo, F. J. *Inorg. Chem.* **1992**, *31*, 1050−1054.
(13) Huang, J. L.; Shang, B. G. *Acta Crystallogr.* **1990**, *Sect. A46 (Suppl.)*, C-287.
(14) Huang, B.; Shang, M.; Huang, J. *Jiegou Huaxue* **1988**, *7* (2), 133−136.
(15) Tremel, W. *Angew. Chem., Int. Ed. Engl.* **1991**, *30*, 840−843.
(16) Tremel, W. *J. Chem. Soc., Chem Commun.* **1991**, 1405−1407.
(17) Neuhausen, J.; Stork, K.-L.; Potthoff, E.; Tremel, W. *Z. Naturforsch.* **1992**, *47b*, 1203−1212.
(18) Neuhausen, J.; Tremel, W. *J. Alloys Comp.* **1994**, *204*, 215−221.
(19) Tremel, W. *Angew. Chem., Int. Ed. Engl.* **1993**, *32*, 1752−1755.
(20) Neuhausen, J.; Tremel, W. *Proceedings: Soft Chemistry Routes to New Materials*; Neuhausen, J., Tremel, W., Eds.; Trans Tech Publications: Aedermannsdorf, Switzerland, 1994; Vol. 152−153, pp 383.
(21) Tremel, W. *Angew. Chem., Int. Ed. Eng.* **1992**, *31*, 217−220.
(22) Badding, M. E.; Li, J.; DiSalvo, F. J.; Zhou, W.; Edwards, P. P. *J. Solid State Chem.* **1992**, *100*, 313−324.
(23) Neuhausen, J.; Evstafyev, V. K.; Kremer, R. K.; Tremel, W. *Chem. Ber.* **1994**, *127*, 1621−1624.
(24) Neuhausen, J.; Finckh, E. W.; Tremel, W. *Inorg. Chem.* **1995**, *34*, 3823−3825.
(25) Li, J.; Badding, M. E.; DiSalvo, F. J. *J. Alloys Comp.* **1992**, *184*, 257−263.
(26) Rouxel, J.; Evain, M. *Eur. J. Solid State Inorg. Chem.* **1994**, *31*, 683−695.
(27) Keane, P. M.; Ibers, J. A. *Inorg. Chem.* **1991**, *30*, 1327−1329.
(28) Cody, J. A.; Ibers, J. A. *Inorg. Chem.* **1994**, *33*, 2713−2715.
(29) Mar, A.; Ibers, J. A. *J. Am. Chem. Soc.* **1993**, *115*, 3227−3238.
(30) Haneveld, A. J. K.; Jellinek, F. *Recl. Trav. Chim. Pays-Bas* **1964**, *83*, 776−783.
(31) Onken, H.; Vierheilig, K.; Hahn, H. *Z. Anorg. Allg. Chem.* **1964**, *333*, 267−279.
(32) Barthelat, J.-C.; Jeannin, Y.; Rancurel, J.-F. *C. R. Acad. Sci. Paris* **1969**, *268*, 1756−1759.
(33) Barthelat, J. C.; Jeannin, Y. *J. Less-Common Met.* **1972**, *26*, 273−283.

S0020-1669(97)00907-5 CCC: $15.00
Published on Web 01/22/1998

isostructural quasi-ternary zirconium tellurides,[34] and a quaternary telluride, $Cs_2Ag_2ZrTe_4$,[35] have also been reported.

In an early study of the ternary Ta−S−C system, the layered compound Ta_2S_2C was discovered.[36] This compound is isostructural with Bi_2Te_2S (Tetradymite)[1] and both 1T and 3R stacking variants are known. Isoelectronic zirconium carbide halides, 1T-Zr_2X_2C (X = Cl, Br), have also been reported.[37] 1T- and 3R-Ta_2S_2C are capable of intercalating nearly all the 3d transition metals,[38] alkali metals,[39] and neutral organic amines[40] and can undergo reversible topotactic intercalation by several cationic species via electrochemical reactions.[41] During our investigation of ternary zirconium tellurides incorporating the post-transition metals, the title compounds, $Zr_{0.30}ZrTe_2$ and $Zr_{0.29}Zr_2Te_2As$, were obtained and the latter was shown to adopt a stuffed Ta_2S_2C structure. Finally, the discovery of related inclusion compound, $NaZr_2Te_2As$, is presented and we suggest that the [Zr_2Te_2As] layered compounds may offer new opportunities as an electron-donating host material.

Experimental Section

Synthesis. Since the tellurides described herein are sensitive to both moisture and oxygen, the operations described below were performed under nitrogen atmosphere. Zr (99.6%, including 4.5% Hf, Johnson Matthey), As (99.99%, Alfa), Te (99.99%, Johnson Matthey), Sn (99.9%, Baker), and Na (99%, Aldrich) were used as starting materials. A mixture of Zr, Sn, and Te in a molar ratio 1:1:1 with 3 mg of $TeCl_4$ was loaded in a Nb capsule which was in turn sealed in an evacuated silica tube ($\sim 10^{-4}$ Torr). The temperature was uniformly raised from room temperature to 1000 °C over 7 days. The reaction was maintained at 1000 °C for 30 days after which the furnace was turned off and allowed to cool to room temperature. Microprobe analysis (Cameca SX-50) on selected crystals showed the composition $Zr_{1.28(2)}Te_2$. No other elements heavier than Na were found. Quantitative synthesis of $Zr_{1.3}Te_2$ can be achieved in either a silica tube or a Nb capsule by mixing stoichiometric proportions of Zr and Te followed by slowly increasing temperature to 800 °C for 24 h and maintaining that temperature for 5 days. The reaction vessels are then quenched to room temperature.

$Zr_{0.29}Zr_2Te_2As$ was synthesized by loading a 1:1:1 ratio of Zr−As−Te with an eutectic LiCl/KCl flux (Zr:Cl ratio = 1:2) in a sealed Nb capsule which was in turn sealed in an evacuated ($\sim 10^{-4}$ torr) and flame-baked silica tube. The temperature of the reaction vessel was uniformly raised to 550 °C over 2 days, maintained at that temperature for 4 days, then uniformly raised to 1000 °C over 4 days, held at that temperature for 3 weeks, and finally cooled to room temperature at a rate of 5 °C/h. The preheating interval at 550 °C helps to reduce the attack of the Nb tubes by Te vapor. The microcrystalline product contained approximately ~60% $Zr_{0.29}Zr_2Te_2As$, the remainder being ZrAs.[42] Single crystals were obtained by cycling the reaction temperature between 1000 and 950 °C repeatedly over a 6 week period. This method produces highly reflective, black, hexagonal-plate crystals which compose > 90% of the product and are suitable for single-crystal, X-ray studies. Selected plate crystals were analyzed by wavelength dispersive X-ray spectrometry which gave the approximate composition $Zr_{2.29(2)}Te_2As_{1.09(4)}$. No contamination by the flux or niobium could be detected.

The inclusion compounds $Na_xZr_2Te_2As$ were synthesized by loading elemental Na, Zr, Te, and As in a ratio of x:2:2:1 (x = 0.1, 0.3, 0.5, 0.7, 0.9, 1.0) in welded Nb capsules which were in turn sealed in evacuated and flame-baked silica tubes. The temperature profile for these reactions was the same as that described for the synthesis of $Zr_{0.29}Zr_2Te_2As$ except that these reactions were maintained at 1000 °C for 2 weeks.

X-ray Studies. General Methods. All synthesized materials were subject to Guinier powder diffraction measurements. Lattice parameters were obtained at room temperature by least-squares refinement of indexed line positions calibrated by an internal silicon standard (NIST). Single-crystal diffraction data for $Zr_{0.30}ZrTe_2$ and $Zr_{0.29}Zr_2Te_2As$ were collected on a Siemens R3m/V diffractometer with graphite-monochromated Mo Kα radiation at 20 °C. Cell constants and an orientation matrix for $Zr_{0.30}ZrTe_2$ were obtained from a least-squares refinement using the setting angles from nine centered reflections. For $Zr_{0.29}Zr_2Te_2As$, preliminary oscillation and Weissenberg photos were used to establish the hexagonal unit cell and to obtain approximate lattice parameters. Unit cells were refined by centering on more than 20 reflections in the range of $15 < 2\theta < 35°$. Cell parameters in Table 1 are refined from Guinier powder diffraction patterns. Intensity data were collected by use of $\theta-2\theta$ scans for reflections with $2\theta < 50°$. In both cases, three check reflections monitored throughout the process of data collection, showed no significant trends.

$Zr_{0.30}ZrTe_2$. A black needle shaped crystal of $Zr_{0.30}ZrTe_2$ having approximate dimensions 0.08 × 0.06 × 0.41 mm was mounted in a glass capillary. After preliminary steps described above were performed, a hemisphere of data were collected ($+h,\pm k,\pm l$) to gain the advantage of averaging. The data were corrected for absorption using the ψ-scan technique based on three reflections. Systematic absences reduced the possible space groups to $P6_3mc$ (No. 186) and $P6_3/mmc$ (No. 194). Guinier diffraction data had made it clear that $Zr_{0.30}ZrTe_2$ is isostructural with the known phase Zr_2Se_3,[43] so the atomic positions of Zr_2Se_3 were used to begin refinement of the $Zr_{0.30}ZrTe_2$ structure.

The structure was refined on F^2 using the SHELX-93 program.[44] Neutral atomic scattering factors, corrected for the real and imaginary parts of anomalous dispersion, were obtained from standard sources.[45] Isotropic refinement of the structure with all Zr and Te positions fully occupied (corresponding to a $Zr_{1.0}ZrTe_2$ composition) resulted in a residual (R) of 6.99%. However, the Zr2 thermal parameter was approximately 100 times larger than that of the Zr1 atom. When the thermal coefficient of the Zr2 atom was constrained to be the same as the Zr1 atom, the isotropic refinement showed that the Zr2 site occupancy factor was 0.30(1) with a residual R = 2.25%. This result is comparable to the composition obtained from microprobe analysis. In subsequent refinement cycles then, both the site occupancy and temperature factor of Zr2 were refined simultaneously which also resulted in reasonable isotropic thermal parameters and a fractional site occupancy of 0.282(6). In the last cycle, the site occupancy of Zr2 was fixed and the structure was refined anisotropically to yield respective residuals of 1.81 and 3.53% for $R_1(F)$ and w$R_2(F^2)$ with $I > 2\sigma(I)$. The largest remaining peaks in the final Fourier difference map were 0.838 and −0.364 e/Å^3 located near Te1 and Zr1 in the framework of the structure.

$Zr_{0.29}Zr_2Te_2As$. A black hexagonal-plate crystal of $Zr_{0.29}Zr_2Te_2As$ with approximate dimensions 0.16 × 0.15 × 0.03 mm was selected and mounted in a glass capillary. After preliminary steps described above were performed, data ranging over the indices ($+h,+k,\pm l$) were collected. Three check reflections were monitored periodically and showed no significant change during the data collection process. The data set was corrected for absorption using the ψ-scan technique based on three reflections. All data except those for which $-h + k + l = 3n$ were found to be absent, consistent with a rhombohedral space group. The structure was solved using direct methods. Refinements in both the space groups $R3m$ (No. 160) and $R\bar{3}m$ (No. 166) yielded essentially

(34) Wang, C.; Hughbanks, T. *Inorg. Chem.* **1995**, *34*, 5224−5229.
(35) Pell, M. A.; Ibers, J. A. *J. Am. Chem. Soc.* **1995**, *117*, 6284−6286.
(36) Beckmann, O.; Boller, H.; Nowotny, H. *Monatsh. Chem.* **1970**, *101*, 945−955.
(37) Hwu, S.-J.; Ziebarth, R.; von Winbush, S.; Ford, J. E.; Corbett, J. D. *Inorg. Chem.* **1986**, *25*, 283−287.
(38) Boller, H.; Sobczak, R. *Monatsh. Chem.* **1971**, *102*, 1226−1233.
(39) Brec, R.; Ritsma, J.; Ouvrard, G.; Rouxel, J. *Inorg. Chem.* **1977**, *16*, 660−665.
(40) Schöllhorn, R.; Weiss, A. *Z. Naturforsch.* **1973**, *28b*, 716−720.
(41) Schöllhorn, R.; Schmucker, W. *Z. Naturforsch.* **1975**, *30b*, 975−977.
(42) Trzebiatowski, W.; Weglowski, S.; Lukaszewicz, K. *Roczniki Chem.* **1958**, *32*, 189−201.
(43) Salomons, W.; Wiegers, G. A. *Recl. Trav. Chim. Pays-Bas* **1968**, *87*, 1339−1344.
(44) Sheldrick, G. M. *SHELXTL-93 User Guide. Crystallography Department, University of Göttingen, Germany, 1993*, 3.4 ed.; Sheldrick, G. M., Ed.; Nicolet Analytical X-ray Instruments: Göttingen, Germany, 1993.
(45) Ibers, J. A.; Hamilton, W. C. *International Tables for X-ray Crystallography*; Kynoch Press: Birmingham, England, 1974; Vol. IV.

Table 1. Crystallographic Data for $Zr_{0.3}ZrTe_2$ and $Zr_{0.29}Zr_2Te_2As$

chem formula	$Zr_{0.3}ZrTe_2$	$Zr_{0.29}Zr_2Te_2As$
a, Å	3.9840(3)	3.9329(4)
c, Å	13.366(3)	29.564(5)
V, Å^3	183.73(7)	396.0(2)
Z	2	3
fw	373.79	539.01
space group	$P6_3mc$ (No. 186)	$R\bar{3}m$ (No. 166)
T (°C)	20	20
λ (Å)	0.71	0.71
ρ_{calcd}, g/cm^3	6.757	6.780
μ (mm^{-1})	19.084	21.359
$R_1(F)^a$ (%)	1.81	1.82
$wR_2(F^2)^b$ (%)	3.53	4.70

^{a} $R_1(F) = \sum(|F_o| - |F_c|)/\sum(|F_o|)$. ^{b} $wR_2(F^2) = [\sum|w(F_o^2 - F_c^2)^2|/\sum|w(F_o^2)^2|]^{1/2}$, $w = 1/[\sigma^2(F_o^2) + (xP)^2 + yP]$, where $P = (\max(F_o^2,0) + 2F_c^2)/3$.

Table 2. Atomic Coordinates and Equivalent Isotropic Displacement Parameters

	x	*y*	*z*	$U_{eq}{}^a$ (Å^2 × 10^3)
			$Zr_{0.3}ZrTe_2$	
Zr1	1/3	2/3	0.3681(1)	17(1)
Zr2	1/3	2/3	0.1009(3)	8(1)
Te1	2/3	1/3	0.2343(1)	12(1)
Te2	0.0	0.0	0.0	19(1)
			$Zr_{0.29}Zr_2Te_2As$	
Zr1	1/3	2/3	0.0488(1)	13(1)
Zr2	1/3	2/3	1/6	19(2)
Te1	2/3	1/3	0.1116(1)	13(1)
As1	0.0	0.0	0.0	9(1)

^{a} Equivalent isotropic *U* defined as one-third of the trace of the orthogonalized $\mathbf{U}_{ij}$ tensor.

the same results, so the centrosymmetric space group $R\bar{3}m$ was chosen for further crystallographic analysis.

The structure refinements were based on F^2 with the use of the SHELX-93 program. Isotropic refinement of $Zr_{0.29}Zr_2Te_2As$ showed reasonable thermal coefficients for all atoms except the Zr2 atom. The Zr2 thermal coefficient was about 91 times larger than that of Zr1, and a residual $R = 10.0\%$ was obtained. When the Zr2 thermal coefficient was constrained to be the same as for Zr1, the isotropic refinement showed that the site occupancy factor was 0.28(1) with a residual $R = 2.67\%$. This result is comparable to the composition obtained from microprobe analysis. In subsequent refinement cycles, both the site occupancy and temperature factor of Zr2 were refined simultaneously which also resulted in reasonable isotropic thermal parameters and a fractional site occupancy of 0.29(1). In the last cycle, the site occupancy of Zr2 was fixed and the structure was refined anisotropically yielding the final respective residuals of 1.82 and 4.70% for $R_1(F)$ and $wR_2(F^2)$ with $I > 2\sigma(I)$. The largest remaining peak in the final Fourier difference map was 1.39 Å away from the Zr1 position. A summary of crystal and data collection parameters of $Zr_{0.30}ZrTe_2$ and $Zr_{0.29}Zr_2Te_2As$ is provided in Table 1, and final atomic coordinates are located in Table 2.

$Na_xZr_2Te_2As$. Because single crystals of $Na_xZr_2Te_2As$ could not be obtained, the crystal structure was determined by powder X-ray diffraction. Step-scanned X-ray powder diffraction data were collected by means of a Rigaku (RU200R) computer-automated diffractometer. The X-ray source was a rotating anode operating at 50 kV and 180 mA with a Cu target and graphite-monochromated radiation. In an attempt to reduce preferred orientation, the samples were mixed with amorphous silica that was dried under vacuum at 500 °C for 1 day. In a nitrogen-filled glove-box, samples were loaded into a chamber designed for use with air−moisture sensitive samples. The chamber is fitted with a Mylar film window and allows a dry nitrogen flow during data collection. Without this sample holder, data collection on these highly air- and moisture-sensitive samples would not be possible. A larger correction for zero-point error is made within the refinement when this sample chamber is employed. The use of this sample chamber reduces the accuracy of the lattice constants obtained, but Guinier film data (for which a primary standard is used) provide the most accurate lattice parameters in any case. The data were collected between 3 and 85° in 2θ with a step size of 0.01° and count time of 6 s/step.

Multiphase Rietveld refinements of the samples with a nominal composition $Na_xZr_2Te_2As$, where $x = 0.5$, 0.7, and 1.0, were carried out using the program GSAS.[46,47] The starting structural model for the Zr_2Te_2As layers in this refinement were obtained from the single-crystal structure of $Zr_{0.29}Zr_2Te_2As$. The compound with a nominal composition $Na_{1.0}Zr_2Te_2As$ was used in these refinements. Lattice parameters and atom positions of the known impurity phases, Na_2Te[48] and ZrAs,[42] were obtained from the literature. Initial isotropic thermal parameters of Zr, Te, and As were obtained from $Zr_{0.29}Zr_2Te_2As$. Initial structural analysis involved the refinements of the zero-point error, scale factor, polarizability factor, lattice parameters, preferred orientation factor, terms for background, peak shape functions, and phase fractions (3.5% Na_2Te and 4.1% ZrAs). Structural parameters of Zr, Te, and As were introduced and refined to yield a layer structure quite comparable to $Zr_{0.29}Zr_2Te_2As$. A difference Fourier map computed at this stage revealed the position of sodium atoms. Sodium atoms were introduced (initial isotropic thermal parameters for sodium were taken from $NaCuZrTe_3$).[49] The Na position was refined together with those of Zr and Te. In the next cycle, the occupancy of sodium ions was refined and a value of 0.99(3) was obtained. A difference Fourier map computed at this stage yielded remnant peaks close (1−2 Å) to Zr, Te, and As. As an internal check refinements of the occupancies of Zr, Te, and As atoms were sequentially performed and gave values were close to 1.0, so the occupancies of these atoms were returned to 1.0. Isotropic thermal parameters of all the atoms were then refined. The final difference plots for $NaZr_2Te_2As$ are given in Figure 1. A summary of data collection and refinement parameters appears in Table 3, and atom positions are given in Table 4. Neither the addition of amorphous silica to sample nor the GSAS refinement procedure entirely compensated for the severe preferred orientation that is characteristic of this layered material (see the labeled reflections in Figure 1). As a result, reliability factors remained somewhat high.

Electrical Resistivity Measurements. Since $Zr_{0.30}ZrTe_2$ and $Zr_{0.29}Zr_2Te_2As$ are sensitive to air and moisture, resistivity measurements were carried out under an atmosphere of dry nitrogen. Resistivities were measured using a dc four-probe method; contacts were made with silver epoxy (Acme E-solder 3021), and leads from the contacts consisted of 0.05 mm diameter gold wires. Because $Zr_{0.29}Zr_2Te_2As$ crystals exhibit a hexagonal-plate morphology, resistivities were only measured parallel to the *ab*-plane. The measurements were repeated at least twice on separate crystals. Temperature equilibration was checked by carrying out measurements while both cooling and warming over the range 77−300 K. Crystal dimensions necessary to obtain the absolute resistivity were measured with a Zeiss laser scanning microscope (LSM-10). The absolute resistivity of $Zr_{0.29}Zr_2Te_2As$ at 273 K, 8.9×10^{-5} Ω cm, was calculated with measured crystal dimensions 0.09 mm × 0.08 mm × 0.02 mm.

Results and Discussion

Syntheses. Early studies of the binary zirconium chalcogenides produced several new sulfide and selenide compounds.[50−54] Solid solutions of $Zr_{1+x}Te_2$ ($0 < x < 1$)

(46) Rietveld, H. M. *J. Appl. Crystallogr.* **1969**, *2*, 65−71.
(47) Larson, A.; Von Dreele, R. B. *GSAS: General Structure Analysis*; Larson, A., Von Dreele, R. B., Eds.; Los Alamos National Laboratory: Los Alamos, NM, 1994.
(48) Villars, P.; Calvert, L. D. *Pearson's Handbook of Crystallographic Data for Intermetallic Phases*, 3rd ed.; American Society for Metals: Materials Park, OH, 1985; Vol. 1.
(49) Mansuetto, M. F.; Keane, P. M.; Ibers, J. A. *J. Solid State Chem.* **1993**, *105*, 580−587.
(50) Hahn, H.; Harder, B.; Mutschke, U.; Ness, P. *Monatsh. Chem.* **1957**, *292*, 82−96.
(51) Conard, B. R.; Franzen, H. F. *The Chemistry of Extended Defects in Non-Metallic Solids*; Conard, B. R.; Franzen, H. F., Ed.; North-Holland: Amsterdam, 1970; Vol. 1969, pp 207−219.

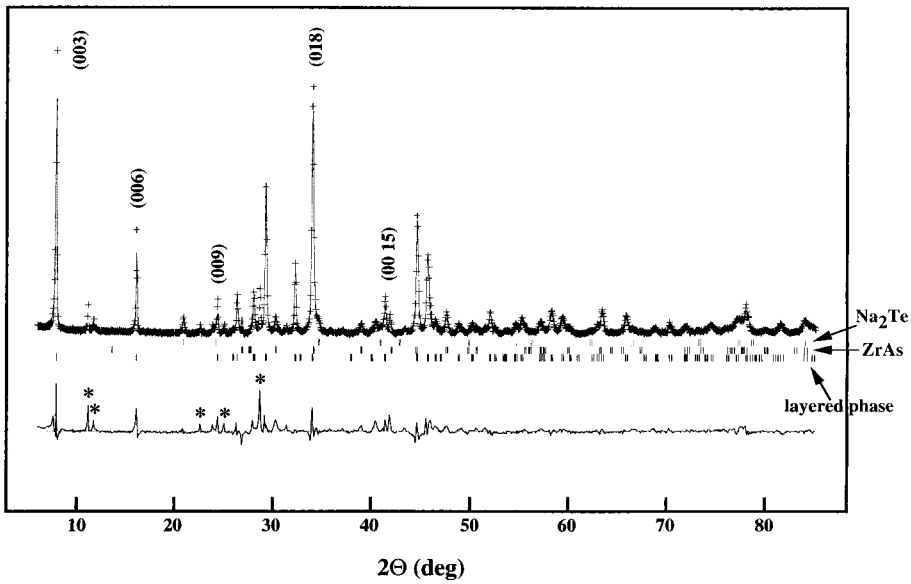

Figure 1. Observed (+) and calculated (−) profiles for the Rietveld refinement of $Na_{0.99(3)}Zr_2Te_2As$. A difference curve is plotted at the bottom. Unidentified reflections, omitted in refinements, are indicated by asterisks on the difference curve. Peaks associated with large *l* and small *h,k* values are labeled.

Table 3. Crystallographic Data for $Na_{0.99(3)}Zr_2Te_2As$

chem formula	$Na_{0.99(3)}Zr_2Te_2As$
a, Å	3.9559(1)
c, Å	32.599(1)
V, Å^3	441.82(3)
Z	3
fw	535.33
space group	$R\bar{3}m$ (No. 166)
T (°C)	20
λ (Å)	1.5406, 1.5444
ρ_{calcd}, g/cm^3	6.036
2θ range, deg	3−85
no. of reflns	7703
no. of structural variables	9
tot. no. of variables	21
R_p[a] (%)	10.95
R_{wp}[b] (%)	14.84
χ^2 [c]	1.893

[a] $R_p = \{\{\sum|y_i(\text{obs}) - y_i(\text{calc})|\}/\sum|y_i(\text{obs})|\}$. [b] $R_{wp} = \{\{\sum w_i(y_i(\text{obs}) - y_i(\text{calc}))^2\}/\sum w_i(y_i(\text{obs}))^2\}^{1/2}$. [c] $\chi^2 = (R_{wp}/R_e)^2$, where $R_e = \{(N-P)/\sum w_i(y_i(\text{obs}))^2\}^{1/2}$.

Table 4. Atomic Coordinates and Isotropic Thermal Parameters of $Na_{0.99(3)}Zr_2Te_2As$

	x	*y*	*z*	U_{eq}[a] (Å$^2 \times 10^3$)
Zr1	$^1/_3$	$^2/_3$	0.04411(8)	13(1)
Na1	$^1/_3$	$^2/_3$	$^1/_6$	30(1)
Te1	$^2/_3$	$^1/_3$	0.09993(6)	11.1(9)
As1	0.0	0.0	0.0	14(2)

[a] Equivalent isotropic *U* defined as one-third of the trace of the orthogonalized $\mathbf{U}_{ij}$ tensor.

showed that compounds adopted either the CdI_2 structure type, when $x < 0.6$, or the NiAs structure type, when $x > 0.6$.[55] McTaggart et al. proposed a "Zr_2Te_3" composition based on the agreement between calculated and measured densities with cell parameters $a = 3.982$ Å and $c = 6.700$ Å (errors were not given).[56] This plausible phase had not been investigated since. During our investigation of the ternary Zr−Sn−Te system, we were able to isolate both $Zr_{0.3}ZrTe_2$ and ZrSnTe.[34] The *a*-axis length determined for $Zr_{0.3}ZrTe_2$ in this study was very nearly that reported by McTaggart et al. for the compound they formulated as "Zr_2Te_3"; however, the *c*-axis length found in that work is about half the value reported here (present work: $a = 3.9840(3)$ Å and $c = 13.366(3)$ Å). Quantitative synthesis of $Zr_{0.3}ZrTe_2$ can be achieved by use of either silica or Nb tubes as containers. The material obtained in silica shows slightly different cell parameters, $a = 3.9706(6)$ Å and $c = 13.365(5)$ Å. In these differences, we are presumably observing the effects of some compositional phase width in $Zr_{1+x}Te_2$, but we have not determined the range over which *x* can be varied.

During our investigation of the ternary Zr−As−Te system, a reaction loaded with elemental Zr, As, and Te in a 1:1:1 ratio and in which a silica tube was used as a container yielded only $Zr_4As_3Te_5$.[57] When the same reaction was attempted in a niobium tube in the presence of a eutectic LiCl/KCl flux, $Zr_{0.29}Zr_2Te_2As$ was obtained serendipitously. We performed the X-ray structure determination discussed herein on a crystal taken from the products of that reaction. When we attempted to prepare a sample of the same compound at the same composition (i.e., $Zr_{0.29}Zr_2Te_2As$), the Guinier powder pattern exhibited slight line shifts (cell parameters: $a = 3.9348(4)$ Å, $c = 29.850(8)$ Å) which suggests that the Zr content may be variable. We have not determined the range over which the Zr content of this phase can be varied. Attempts to synthesize the isostructural sulfide and selenide have been unsuccessful.

$Zr_{0.30}ZrTe_2$. The structure of $Zr_{0.3}ZrTe_2$ is projected approximately along the *a* axis in Figure 2, and important bond distances are listed in the Table 5. $Zr_{0.3}ZrTe_2$ adopts the Ti_2S_3 structure type and is composed of hexagonal $ZrTe_2$ layers which are isostructural with CdI_2.[58,59] Isostructural M_2Se_3 (M = Zr,[43] Hf[60]) have also been reported. The layers are built up with

(52) Stocks, K.; Eulenberger, G.; Hahn, H. *Z. Anorg. Allg. Chem.* **1970**, *374*, 318−325.
(53) Kim, S.-J.; Nguyen, T.-H.; Franzen, H. F. *J. Solid State Chem.* **1987**, *70*, 88−92.
(54) Hahn, H.; Ness, P. *Z. Anorg. Allg. Chem.* **1959**, *302*, 39−49.
(55) Hahn, H.; Ness, P. *Z. Anorg. Allg. Chem.* **1959**, *302*, 136−154.
(56) McTaggart, F. K.; Wadsley, A. D. *Aust. J. Chem.* **1958**, *11*, 445−457.
(57) Mosset, A.; Jeannin, Y. *J. Less-Common Met.* **1972**, *26*, 285−292.
(58) Norrby, L.-J.; Franzen, H. F. *J. Solid State Chem.* **1970**, *2*, 36−41.
(59) Wadsley, A. D. *Acta Crystallogr.* **1957**, *10*, 715−716.
(60) Schewe-Miller, I. M.; Young, V. G. *J. Alloys Comp.* **1994**, *216*, 113−115.

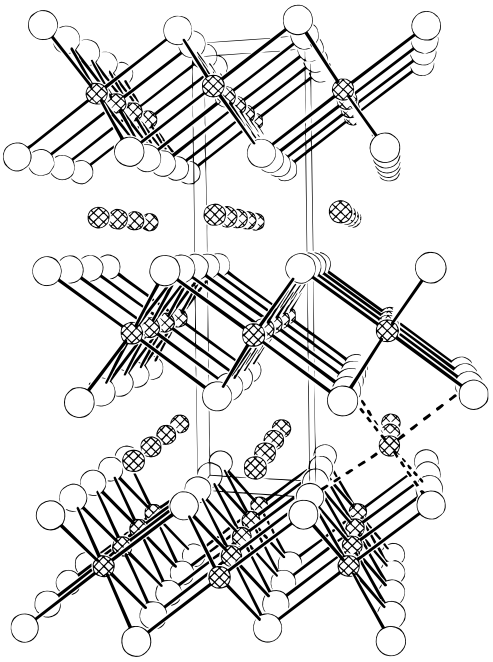

Figure 2. Approximate (100) projection of $Zr_{0.3}ZrTe_2$ structure. The octahedral surroundings of one interlayer Zr atom are indicated with dashed lines. Zr atoms are shown as cross-hatched circles, and Te atoms, as open circles.

Table 5. Important Interatomic Distances (Å) and Bond Angles (deg) for $Zr_{0.3}ZrTe_2$

Zr1−Te1 (3×)	2.913(1)	Zr2−Te1 (3×)	2.910(3)
Zr1−Te2 (3×)	2.890(1)	Zr2−Te2 (3×)	2.666(2)
Zr1−Zr2	3.571(4)	Zr1−Zr2	3.869(3)
Te1−Zr1−Te1	86.27(4)	Te1−Zr2−Te1	86.4(1)
Te1−Zr1−Te2	93.44(2)	Te1−Zr2−Te2	88.22(2)
Te2−Zr1−Te2	86.84(4)	Te2−Zr2−Te2	96.7(1)
Zr1−Te1−Zr2	75.65(6)	Zr1−Te2−Zr2	88.01(5)

fairly regular $ZrTe_6$ octahedra (Zr−Te, 3 × 2.890 and 3 × 2.913 Å). Each of the additional zirconium atoms are included between the CdI_2-like layers to form a distorted $ZrTe_6$ octahedron that shares faces with an octahedron in the layer above and edges with three such octahedra in the layer below. On the face-shared side, zirconium forms three long bonds to tellurium (3 × 2.910(3) Å) and three short bonds on the edge shared side (3 × 2.666(2)). Two Zr−Zr distances (3.571(4) and 3.869(3) Å) respectively result from face- and edge-sharing. The structure of this compound can be described as intermediate between CdI_2 (where the Zr2 site is empty) and TiP (where the same site is fully occupied by Ti).[61] If we make the formal assumption that zirconium atoms which are "included" between slabs are fully oxidized, then metal atoms within the slabs are $Zr^{2.8+}$. This formal assignment is consistent with the difference in Zr−Te distances; the average distance (2.788 Å) between Te and the included Zr is slightly shorter than that in $ZrTe_2$ (2.819 Å) and 0.11 Å shorter than Zr_{slab}−Te distances. Thus, the $[ZrTe_2]$ slabs bear a formal negative charge somewhat greater than unity: $[ZrTe_2]^{1.2-}$. A long Zr−Zr contact distance (3.571 Å) between the included Zr atom and the Zr atom in the slab is observed. In comparison with $Zr_{0.3}ZrTe_2$, the "included" Zr site is fully occupied in ZrAs[42] (≡ $ZrZrAs_2$; TiP-type), both Zr atoms have a formal +3 oxidation state, and the Zr−Zr bond distance is 3.218 Å (Figure 3). The long corresponding Zr−Zr distance in $Zr_{0.3}ZrTe_2$ is the *apparent* result of repulsion between

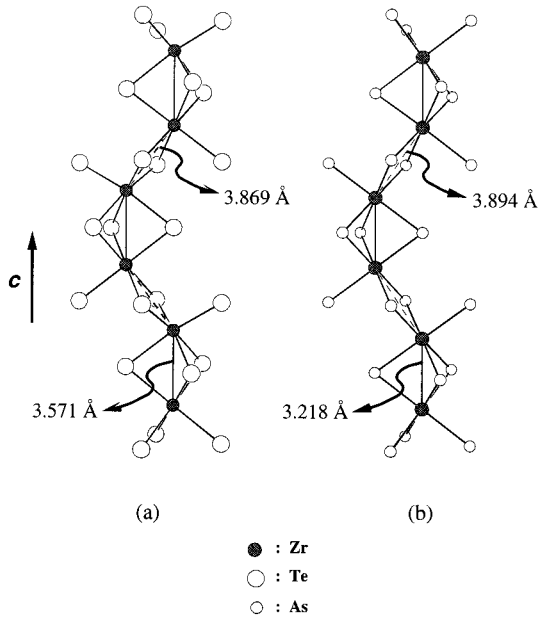

Figure 3. Approximate (100) projection of the Zr−Zr contacts in both $Zr_{0.3}ZrTe_2$ (a) and ZrAs (b) compounds. The asymmetric octahedral environment of Zr atoms is observed in $Zr_{0.3}ZrTe_2$ while that of the ZrAs displays symmetric one.

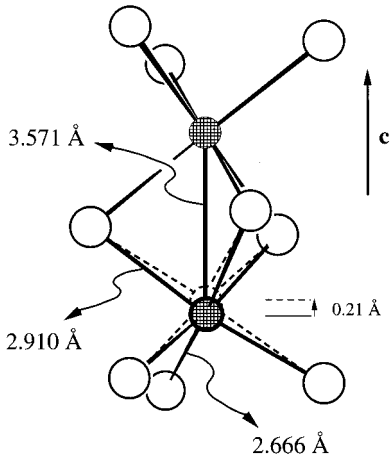

Figure 4. The octahedral coordination environment of the "intercalated" Zr atom is highlighted. Zr atoms are shown as cross-hatched circles, and Te atoms, as open circles. An idealized $ZrTe_6$ octahedron is shown with dashed lines and a circle.

Zr^{4+} and $Zr^{2.8+}$ and is associated with the movement of "included" Zr atoms away from Zr atoms in the slab along the *c* axis by 0.13 Å (compared with an idealized case in which all the Zr−Te distances are equal; see Figure 4) and the concomitant asymmetry in the Zr−Te distances about the included zirconium center.

$Zr_{0.29}Zr_2Te_2As$. A single-crystal structure determination revealed that $Zr_{0.29}Zr_2Te_2As$ (Figure 5) is isostructural with 3R-$M_xTa_2S_2C$, (M = Ti−Ni),[38] a layered material built up with close packed hexagonal layers of anions. Individual slabs in $Zr_{0.29}Zr_2Te_2As$ display a [Te−Zr−As−Zr−Te] stacking sequence. Slabs are stacked such that a rhombohedral structure is obtained; i.e., there are three slabs per hexagonal unit cell. Each Zr in a given layer is bonded to three Te and three As atoms that form a somewhat distorted trigonal antiprism (Zr1−Te, 3 × 2.933 Å; Zr1−As, 3 × 2.691Å), while every As is surrounded by six zirconium atoms which form a flattened, trigonal antiprism (Zr1−As1, 6 × 2.691 Å; six long Zr−Zr distances in triangular faces that lie within Zr layers, 6 × 3.933

(61) Snell, P.-O. *Acta Chem. Scand.* **1967**, *21*, 1773−1776.

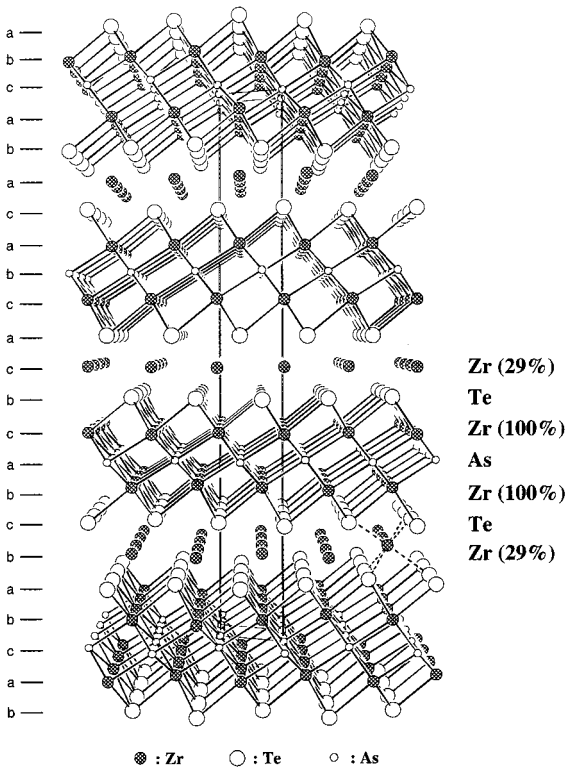

Figure 5. Approximate (100) projection of $Zr_{0.29}Zr_2Te_2As$ structure. The octahedral surroundings of one interlayer Zr atom are indicated with dashed lines. The stacking sequence of hexagonal layers is shown on the left. Labels at right are provided to clarify the layer stacking and occupancies.

Å; six short Zr−Zr contacts between Zr layers within a slab, 6 × 3.673 Å). The shortest Te−Te contact within a layer is 3.933 Å, which indicates no significant bonding. The X-ray refinement indicates that 29% of the trigonal antiprismatic interstices between slabs are occupied by Zr atoms (Zr2−Te1, 6 × 2.794 Å). It should be noted that the closest Zr−Zr contacts in the structure are between these included Zr atoms and Zr centers within the slabs (Zr1−Zr2, 2 × 3.484 Å). Just as Zr_2Cl_2C and Ta_2S_2C can be viewed as condensed cluster compounds of the M_6X_{12} type,[37,62−64] $Zr_{0.29}Zr_2Te_2As$ can be viewed as a unique example of a chalcogenide condensed cluster compound with a $[Zr_6As]$ core.

Electronic Structure of $Zr_{0.29}Zr_2Te_2As$. $Zr_{0.29}Zr_2Te_2As$ is isostructural with a number of halides and chalcogenides: Ta_2S_2C,[36] M_2Cl_2Z (M = Sc, Y, Zr; Z = C, N),[37] M_2X_2C (M = Gd, Lu; X = Cl, Br),[65,66] and Bi_2Te_2S.[1] The valence electron concentrations and metal−metal distances in Zr_2Cl_2C and Ta_2S_2C indicate that metal−metal bonding is of some importance (Ta^{IV} and Zr^{III} are d^1 metals, assuming these are formally ionic carbides). Y_2Cl_2N is also expected to be metallic in accord with the formal electron counting scheme: $(Y^{2.5+})_2(Cl^{1-})_2N^{3-}$. On the other hand, the rare-earth compounds M_2X_2C (M = Sc, Gd, Lu; X = Cl, Br) all have saltlike electronic configurations and are insulating (no extra d electrons to form metal−metal bonds within and between layers). The bismuth oxidation state, Bi−Bi distances, and the electronic structure of bismuth (as a p-block element) all preclude Bi−Bi bonding in Bi_2Te_2S. If we make the formal assumption that zirconium atoms which

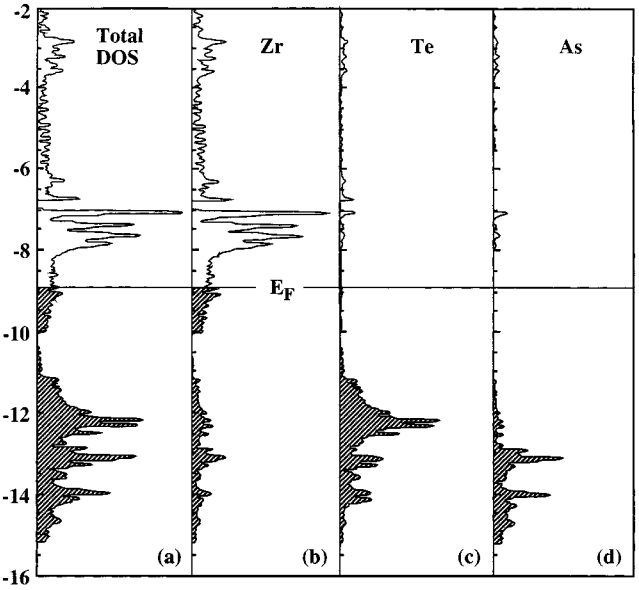

Figure 6. Total density of states (DOS) diagram for a 2-D $[Zr_2Te_2As]^{1.16-}$ layer (a). The projected DOS of Zr (b), Te (c), and As (d) are shown. Filled levels are shaded.

are "included" between slabs are fully oxidized, then metals within the slabs are $Zr^{2.92+}$. As for $Zr_{0.3}ZrTe_2$, this formal assignment is consistent with the difference in Zr−Te distances; Te distances to the "included" Zr are shorter than Zr−Te bonds in $ZrTe_2$ and 0.16 Å shorter than Zr_{slab}−Te distances. Thus, the $[Zr_2Te_2As]$ slabs bear a formal negative charge somewhat greater than unity: $[Zr_2Te_2As]^{1.16-}$.

We have calculated the electronic band structure for a model 2-D $[Zr_2Te_2As]^{1.16-}$ slab using the extended Hückel method.[67,68] The Fermi level lies in the Zr d bands above a gap in the total density of states (DOS) that separates the Zr d bands from the Te and As p bands (Figure 6a). Thus, we anticipate that $Zr_{0.29}Zr_2Te_2As$ will be a metallic conductor. Inspection of the projected DOS curves shows that between −15.0 and −10.0 eV (up to the gap) crystal orbitals are primarily Te and As localized (Figure 6c,d), while the higher lying levels have mainly Zr d character (Figure 6b). There is significant Zr−Te and Zr−As covalency, as evidenced by the mixing of Zr-based orbitals into Te- and As-based manifolds. Of course, the p bands have Zr−Te and Zr−As bonding character, which can be seen by referring to the crystal orbital overlap populations (COOPs), in Figure 7a,b. The zirconium d bands have weak Zr−Zr bonding character up to and a bit beyond the Fermi level (Figure 7c). This figure indicates that the layer can take up a total charge of 3− before all levels with Zr−Zr bonding character are filled. Although the valence electron concentration (VEC) of the $[Zr_2Te_2As]^{1.16-}$ layers is 0.16 electron greater than the VEC for Ta_2S_2C, through-space Zr−Zr bonding is weaker in $Zr_{0.29}Zr_2Te_2As$ than is Ta−Ta bonding in the Ta_2S_2C because in the former compound a much larger atom must be accommodated in the metal octahedral interstice (As vs C).

$Na_xZr_2Te_2As$. Self-intercalated layered materials like $Ta_{1+x}S_2$ were harbingers of a more general class of intercalation compounds, M_xTaS_2 (M = alkali metals and 3d transition metals).[5] In a similar vein, metastable binary phases can sometimes be obtained by oxidative deintercalation of a stable ternary; the formation of layered VS_2 by oxidative deinterca-

(62) Corbett, J. D. *Acc. Chem. Res.* **1981**, *14*, 239−246.
(63) Simon, A. *Angew. Chem., Int. Ed. Engl.* **1981**, *20*, 1−22.
(64) Simon, A. *Angew. Chem., Int. Ed. Engl.* **1988**, *27*, 160−183.
(65) Schwanitz, U.; Simon, A. *Z. Naturforsch* **1985**, *40b*, 710−716.
(66) Schleid, T.; Meyer, G. *Z. Anorg. Allg. Chem.* **1987**, *552*, 90−96.
(67) Hoffmann, R. *J. Chem. Phys.* **1963**, *39*, 1397−1412.
(68) Whangbo, M.-H.; Hoffmann, R. *J. Am. Chem. Soc.* **1978**, *100*, 6093−6098.

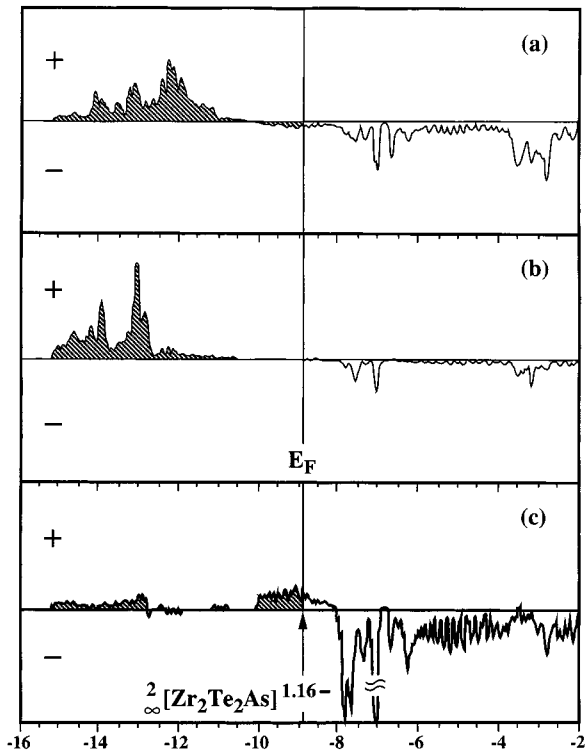

Figure 7. Averaged crystal orbital overlap population (COOP) curves for Zr−Te (a), Zr−As (b), and Zr−Zr (c) contacts less than 2.8, 3.0, and 3.7 Å, respectively. Levels above horizontal axes are bonding (+) while below are antibonding (−). Filled levels are shaded.

Table 6. Cell Parameters (Å) as a Function of Na Content in $Na_xZr_2Te_2As$[a]

Na content	*a*	*c*
1.0	3.9468(7)	32.759(6)
0.9	3.9445(8)	32.77(2)
0.7	3.9431(3)	32.789(5)
0.5	3.9547(7)	32.787(8)

[a] Refined from Guinier powder diffraction patterns using Si as an internal standard.

lation of Li_xVS_2 with I_2 stands as a case in point.[69] The presence of interlayer Zr ions between the [Te−Zr−As−Zr−Te] layers of $Zr_{0.29}Zr_2Te_2As$, the Zr−Zr bonding character of levels surrounding the Fermi level, and analogies with the chemistry of $M^I_xTa_2S_2C$ compounds all suggested that $M^I_xZr_2Te_2As$ compounds might be accessible and prompted us to investigate the existence of $[Zr_2Te_2As]$ layer compounds containing alkali metals. The synthesis of inclusion compounds $Na_xZr_2Te_2As$ (x = 0.1, 0.3, 0.5, 0.7, 0.9, 1.0) was attempted by mixing elemental Na, Zr, Te, and As in stoichiometric proportions and heating at 1000 °C for 2 weeks. For $x \geq 0.5$, the reaction product was predominantly $Na_xZr_2Te_2As$, though some unidentified lines in the Guinier diffraction pattern indicated that the synthesis was not quantitative. The yield can be made virtually quantitative if one is persistent in grinding and reheating the product at temperatures in the 900 °C range for an additional 1 week. Cell parameters obtained from the Guinier powder diffraction patterns of all the reaction products with $x \geq 0.5$ are listed in Table 6. These results show slight variations in both *a* and *c* axis lengths, but no clear trends are evident. No Na-containing layered compound could be detected for $x \leq 0.3$, implying that the minimum stable Na loading in $Na_xZr_2Te_2As$ is $x > 0.3$.

Rietveld refinements were carried out to determine the sodium contents and structure of $Na_xZr_2Te_2As$. Problems associated with the existence of unknown impurities, preferred orientation, and moisture sensitivity of $Na_xZr_2Te_2As$ limited the quality of powder X-ray data. Nevertheless, we were able to obtain a reasonable structural information from these refinements. Sodium contents of the compounds with the nominal composition $Na_xZr_2Te_2As$, where $x = 0.5$, 0.7, and 1.0, were calculated from the Rietveld refinements as 0.67(2), 0.83(3), and 0.99(3), respectively. The latter phase is the most completely analyzed to date, and only for that phase do we present detailed results here. The $Na_xZr_2Te_2As$ phases were found to be isostructural with the related $Zr_{0.29}Zr_2Te_2As$ compound. Structural details of the other compounds will be published elsewhere. The Zr_2Te_2As layers in $NaZr_2Te_2As$ remain much as they are in the parent ternary compound (Zr−Te, 3 × 2.918(2) Å, and Zr−As, 6 × 2.700(1) Å) with a 0.1 Å decrease in thickness relative to that of $Zr_{0.29}Zr_2Te_2As$ (layer thickness = 6.6 Å). Sodium ions are bonded to six Te atoms forming a trigonal antiprism (Na−Te, 6 × 3.155(1) Å). The Na−Te, Zr−As, and Zr−Te distances in $NaZr_2Te_2As$ are comparable to those of Na_2Te (Na−Te, 8 × 3.158 Å)[48] and $Zr_{0.29}Zr_2Te_2As$. The spacing separating Te layers of adjacent slabs (i.e. interlayer distance) in $Zr_{0.29}Zr_2Te_2As$ is 3.25 Å but increases to 4.37 Å in $NaZr_2Te_2As$. The 1.12 Å increase in the interlaminar distance is not uncommon for Na-intercalated layered transition metal sulfides;[70] for example, an increase of 1.2 Å is observed on moving from Ta_2S_2C to $Na_{0.15}Ta_2S_2C$.[39] Notably, the rhombohedral stacking observed in 3R-$Na_xZr_2Te_2As$ differs from the 2H-type stacking found in $Na_xTa_2S_2C$ ($0 < x < 1$). The latter compounds (with two Ta_2S_2C slabs per unit cell) were found when sodium was intercalated into Ta_2S_2C at −77 °C by reaction with Na/NH_3.[39]

The synthesis of $Na_xZr_2Te_2As$ raises questions of whether such a compound can be deintercalated and whether Zr_2Te_2As-based layered materials might be accessible via ion-exchange reactions. Preliminary experiments suggest sodium ions can be exchanged to form $Li_xZr_2Te_2As$. We defer further discussion to future publications.

Resistivity Measurements. The extended network structures and fractional electron counts of $Zr_{0.30}ZrTe_2$ and $Zr_{0.29}Zr_2Te_2As$ lead us to expect metallic conductivity for these compounds. Four-probe single-crystal resistivity measurements show that both $Zr_{0.30}ZrTe_2$ and $Zr_{0.29}Zr_2Te_2As$ compounds do indeed show metallic behavior throughout the temperature range 77−300 K (Figure 8). This metallic behavior is also consistent with the results from the extended Hückel calculations of the $Zr_{0.29}Zr_2Te_2As$. The room-temperature resistivity of the $Zr_{0.29}Zr_2Te_2As$ is fairly low, 8.9×10^{-5} Ω cm (273 K), compared with other metal-rich chalcogenides we have recently studied.[34,71−73] Assuming we can extrapolate the temperature-dependent data back to 0 K, the large low-temperature residual resistivity should persist, probably reflecting the effects of defect scattering associated with disorder of the included Zr atoms and grain boundary scattering.

(69) Murphy, D. W.; Cross, C.; DiSalvo, F. J.; Waszczak, J. V. *Inorg. Chem.* **1977**, *16*, 3027−3031.

(70) Rouxel, J. *Intercalated Layered Materials*; Rouxel, J., Ed.; Reidel: Dordrecht, Holland, 1979; Vol. 6, pp 201−250.

(71) Ahn, K.; Hughbanks, T. *J. Solid State Chem.* **1993**, *102*, 446−454.

(72) Ahn, K.; Hughbanks, T.; Rathnayaka, K. D. D.; Naugle, D. G. *Chem. Mater.* **1994**, *6*, 418−423.

(73) Wang, C. C.; Abdon, R. L.; Hughbanks, T.; Reibenspies, J. *J. Alloys Comp.* **1995**, *226*, 10−18.

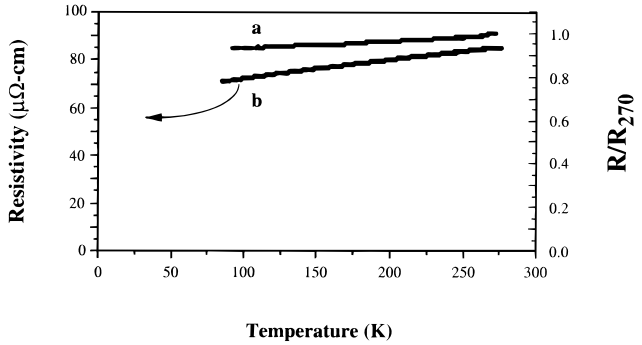

Figure 8. Single-crystal temperature dependent resistivities of $Zr_{0.3}ZrTe_2$ (a) and $Zr_{0.29}Zr_2Te_2As$ (b) are shown. No absolute resisitivity is available for $Zr_{0.3}ZrTe_2$, and only the temperature dependence of the measured resistance is given.

Concluding Remarks. The layered compounds $Zr_{0.30}ZrTe_2$, $Zr_{0.29}Zr_2Te_2As$, and $Na_xZr_2Te_2As$ have been synthesized and characterized by the use of single-crystal and powder X-ray diffraction, microprobe analysis, and electrical resistivity measurements. We consider the discovery of the latter two Ta_2S_2C-type structures to be of particular interest and believe that the sodium-intercalated phase may open up new topochemical opportunities in a relatively unexplored chemical context. While porous layered and network compounds that can serve as hosts to electron donors (cations) are relatively abundant, the number of materials that might serve as hosts to acceptors is much smaller and those which have demonstrated such behavior require fairly powerful oxidants (e.g., graphite).[74] The prospect of developing new chemistry wherein Zr_2Te_2As-based layers serve both as host and reducing agent to guest acceptors serves to motivate research now underway in our laboratory.

Acknowledgment. This research was generously supported by the National Science Foundation through Grant DMR-9215890 and by the Robert A. Welch Foundation through Grant A-1132. The R3m/v single-crystal X-ray diffractometer and crystallographic computing system were purchased from funds provided by the National Science Foundation (Grant CHE-8513273). We thank Dr. Damadora Poojary for his assistance with powder X-ray diffraction data collection and Prof. Abraham Clearfield for generous access to facilities in his laboratories. We also thank Dr. Renald Guillemette for his assistance with the microprobe analyses.

Supporting Information Available: Tables of anisotropic displacement parameters for $Zr_{0.30}ZrTe_2$ and $Zr_{0.29}Zr_2Te_2As$ (2 pages). Ordering information is given on any current masthead page.

IC9709077

(74) Müller-Warmuth, W.; Schöllhorn, R. *Progress in Intercalation Research*; Müller-Warmuth, W., Schöllhorn, R., Eds.; Kluwer Academic Publishers: Dordrecht, The Netherlands, 1994; Vol. 17, pp 83−176.